

# Model independent tests of the Kerr bound with extreme mass ratio inspirals

Gabriel Andres Piovano<sup>1</sup>, Andrea Maselli<sup>1</sup>, Paolo Pani<sup>1</sup>

<sup>1</sup> *Dipartimento di Fisica, “Sapienza” Universit di Roma & Sezione INFN Roma1, Piazzale Aldo Moro 5, 00185, Roma, Italy*

An outstanding prediction of general relativity is the fact that the angular momentum  $S$  of an isolated black hole with mass  $\mu$  is limited by the Kerr bound,  $S \leq G\mu^2/c$ . Testing this cornerstone is challenging due to the difficulty in modelling spinning compact objects that violate this bound. We show that precise, model-independent tests can be achieved by measuring gravitational waves from an extreme mass ratio inspiral around a supermassive object, one of the main targets of the future LISA mission. In the extreme mass ratio limit the dynamics of the small compact object depends on its multipole moments, but not on the details of its structure. Thus, its spin is a free parameter and can exceed the Kerr bound. By computing the orbital dephasing and the gravitational-wave signal emitted by a generically spinning point particle in circular, equatorial motion around a Kerr black hole, we estimate that LISA will be able to measure the spin of the small compact object at the level of 10%, also allowing for theory-agnostic, unprecedented constraints on string-theory inspired objects such as “superspinars”, almost in their entire parameter space.

**Introduction.** The dawn of black-hole (BH) physics can be arguably traced back to the seminal work by Penrose [1, 2], Wheeler [3], Hawking [4], Bekenstein [5, 6], Carter [7, 8], and many others during the first “golden age” of General Relativity in the 1970s. Since then, the field has evolved dramatically and several theoretical predictions have been experimentally confirmed to exquisite precision [9–11]. Nonetheless, some basic relativistic effects associated with BHs remain elusive and have not been yet tested directly.

Arguably the most striking one is the fact that a BH with mass  $\mu$  can spin only below a critical value<sup>1</sup> of the angular momentum  $S$ ,

$$|S| \leq S_{\max} \equiv \frac{G\mu^2}{c} \approx 2 \times 10^{44} \left( \frac{\mu}{15M_{\odot}} \right)^2 \text{ kg m}^2/\text{s}, \quad (1)$$

above which a naked singularity would appear. This is a consequence of the uniqueness of the Kerr metric, which is regular outside an event horizon only if the above “Kerr bound” is fulfilled.

Testing the Kerr bound is challenging [13–17]. The standard route is to interpret observations in various contexts *assuming* the Kerr metric and look for inconsistencies in explaining the data. This strategy is not optimal as one would wish to compare the Kerr case with some alternative and perform Bayesian model selection. The latter option is however hampered by the fact that the geometry of spinning BHs beyond general relativity [14] – or of spinning extreme compact objects without a horizon [17] (such as boson stars) – is known only perturbatively or numerically [18–27]. Furthermore, regardless of the technical difficulties, any analysis based on a specific

model or theory would be limited to that specific case, whereas performing a *model-independent* test of the Kerr bound (1) would be much more profitable.

In this letter and in a companion technical paper [28], we show that such model-independent tests of the Kerr bound can be achieved with extreme mass ratio inspirals (EMRIs). EMRIs are one of the main targets of the future space-based Laser Interferometer Space Antenna (LISA) [29] and of evolved concepts thereof [30]. Owing to the large number of gravitational-wave (GW) cycles, EMRI signals detectable by LISA can be used to extract the binary parameters with exquisite accuracy [31], and to perform unique tests of fundamental physics [31–41] (see [16, 42] for some recent reviews).

**Setup.** In an EMRI a small, stellar-size, compact object (dubbed as secondary) of mass  $\mu$  orbits around a supermassive object (dubbed as primary) of mass  $M \sim (10^6 \div 10^9)M_{\odot}$ ; the typical mass ratio of the system is  $q = \mu/M \in (10^{-7} \div 10^{-4})$  and therefore allows for a small- $q$  expansion of Einstein’s equations. To the leading order in  $q$ , the dynamics is described by a point particle of mass  $\mu$  in motion around the primary. The orbits evolve quasi-adiabatically through a sequence of geodesics due to energy and angular momentum loss carried away by GWs [43, 44]. To higher order in a small- $q$  expansion, the dynamics remains oblivious to the specific nature of the secondary, which can still be described by a point particle endowed with a series of multipole moments. The next-to-leading order correction depends on conservative self-force effects [44] and also on the intrinsic angular momentum  $S$  of the secondary, which is the main target of our investigation. It is convenient to introduce the dimensionless spin parameter of the secondary,

$$\sigma \equiv \frac{S}{\mu M} = \chi q, \quad (2)$$

where  $\chi \equiv S/\mu^2$  is the reduced spin of the secondary. Owing to the mass ratio dependence, for an EMRI  $|\sigma| \ll 1$  provided  $|\chi| \ll 1/q$ . In order to test the Kerr bound (1)

<sup>1</sup> As a reference, the angular momentum of the fastest spinning pulsar is about  $10^{42} \text{ kg m}^2/\text{s}$ . However the normalized bound,  $S_{\max}/\mu^2 = 1$  (in  $G = c = 1$  units henceforth adopted [12]), is very modest: a solid ball of mass 1 kg and radius 10 cm making one revolution per second has  $S/\mu^2 \sim 10^{17}$ .

we can study the EMRI evolution in which the secondary is assumed to be either a Kerr BH, which fulfills the constraint  $|\chi| \leq 1$ , or an extreme compact object [17] that can violate such a bound, i.e.  $|\chi| > 1$ . Occasionally these objects are called *superspinars* and were suggested to arise generically in high-energy modifications to general relativity such as string theories [45]. Remarkably, we do not need to make any assumption on the specific properties of these objects, and we will show how GW signals detectable by LISA are potentially able to perform smoking gun, theory-agnostic tests of the Kerr bound solely based on a measurement of  $\chi$ .

High-curvature corrections for the primary are negligible compared to the secondary [46]. Therefore, we assume that the background spacetime is described by the Kerr metric given, in Boyer-Lindquist coordinates, by

$$ds^2 = -dt^2 + \Sigma(\Delta^{-1}dr^2 + d\theta^2) + (r^2 + a^2)\sin^2\theta d\phi^2 + 2Mr/\Sigma(a\sin^2\theta - dt)^2, \quad (3)$$

where  $\Delta = r^2 - 2Mr + a^2$ ,  $\Sigma = r^2 + a^2\cos^2\theta$ , and  $a$  is the spin parameter of the primary such that  $|a| \leq M$ .

The dynamics of the spinning point particle on the Kerr background can be obtained through the covariant conservation of the energy-momentum tensor leading to the Mathisson-Papapetrou-Dixon equations of motion [47–54]. We integrate such equations supplied by the Tulczyjew-Dixon condition,  $S^{\mu\nu}p_\nu = 0$ , between the spin tensor  $S^{\mu\nu}$  and the body 4-momentum  $p^\mu$  [55]. This constraint fixes the center of mass reference frame, and guarantees that the squared mass  $\mu^2 = -p_\mu p^\mu$  and spin magnitude  $S^2 = \frac{1}{2}S_{\mu\nu}S^{\mu\nu}$  are conserved during the orbital evolution. The equations of motions are valid as long as  $(S/\mu)^2 \ll |R_{\mu\nu\rho\sigma}|^{-1}$  [56], namely if the size of the spinning secondary is much smaller than the background curvature radius specified by the Riemann tensor  $|R_{\mu\nu\rho\sigma}|$ . For the Kerr spacetime,  $|R_{\mu\nu\rho\sigma}| \sim M/r^3$ , and the validity condition of the equations of motion requires

$$\left(\frac{r}{M}\right)^3 \gg \left(\frac{S}{\mu M}\right)^2 = \sigma^2, \quad (4)$$

which is always satisfied for EMRIs since  $\sigma \ll 1$ .

During its motion the secondary acts as a perturbation of the background spacetime. GW emission from the binary can be computed using the Teukolsky formalism for spin  $s = -2$  perturbations, described by the invariant Weyl scalar [57, 58]. The radial component  $R_{\ell m \omega}(r)$  of the latter satisfies the wave-like equation

$$\Delta^2 \frac{d}{dr} \left( \frac{1}{\Delta} \frac{dR_{\ell m \omega}}{dr} \right) - V_{\ell m \omega}(r) R_{\ell m \omega} = \mathcal{T}_{\ell m \omega}(r), \quad (5)$$

for any integer  $\ell \geq 2$  and  $|m| \leq \ell$ . The effective potential  $V_{\ell m \omega}(r)$  is given in Ref. [44], whereas the source term  $\mathcal{T}_{\ell m \omega}(r)$  depends on the stress-energy tensor of the secondary. The latter depends explicitly on the spin  $\sigma$  in

two ways: directly, since the spin of the secondary affects the energy content of the source, and indirectly through the trajectory of the secondary, which is affected by spin-angular momentum couplings. The final expression is cumbersome and derived in detail in Ref. [28].

**GW flux.** We numerically integrate Eq. (5) using a standard Green function approach [28]. We first solve the homogeneous problem (with two different methods [28]) finding the solution  $R_{\ell m \omega}^-$  (resp.,  $R_{\ell m \omega}^+$ ) that satisfies suitable boundary conditions of ingoing (resp., outgoing) radiation at the horizon (resp., infinity). The full solution  $R_{\ell m \omega}(r)$  is then obtained by convoluting the homogeneous solutions with the source terms. Asymptotically the amplitude of the wave  $R_{\ell m \omega}(r)$  is

$$Z_{\ell m \omega}^\pm = C_{\ell m \omega}^\pm \int_{r_\pm}^\infty \frac{R_{\ell m \omega}^\mp(r') \mathcal{T}_{\ell m \omega}(r')}{\Delta(r')^2} dr', \quad (6)$$

where the upper (lower) sign refers to the outgoing (ingoing) wave at infinity (horizon), and  $C_{\ell m \omega}^\pm$  are some constant coefficients [28, 58].

For simplicity we focus on circular, equatorial orbits and – to avoid precession [59] – assume that the spin of the secondary is (anti)aligned with that of the primary. Extensions to more generic orbits are conceptually straightforward and should not affect the order of magnitude of our constraints. For circular orbits the source has a discrete spectrum, such that  $Z_{\ell m \omega}^\pm = Z_{\ell m}^\pm \delta(\omega - m\Omega)$ , with  $\Omega$  being the orbital frequency [59]

$$\Omega = \frac{\delta E}{\delta J_z} = \frac{\partial E}{\partial r} \left( \frac{\partial J_z}{\partial r} \right)^{-1}, \quad (7)$$

where  $E$  and  $J_z$  are constants of motion that can be interpreted at infinity as the particle’s energy and *total* angular momentum along the  $z$ -axis. Introducing the rescaled quantities  $\hat{E} = E/\mu$ ,  $\hat{J}_z = J_z/(\mu M)$ ,  $\hat{r} = r/M$ , and  $\hat{a} = a/M$  we find [28]

$$\hat{E} = [\hat{r}\sqrt{\Delta} + (\hat{a}\hat{r} + \sigma)U_\mp]n^{-1}, \quad (8)$$

$$\hat{J}_z = [\hat{r}\sqrt{\Delta}(\hat{a} + \sigma) + U_\mp(\hat{r}^3 + \hat{r}\hat{a}(\hat{a} + \sigma) + \hat{a}\sigma)]n^{-1}, \quad (9)$$

where  $n = \hat{r}^2\sqrt{1 - U_\mp^2}$ , with the  $\mp$  sign corresponding to co-rotating and counter-rotating orbits, respectively (henceforth we focus on the former orbits). The form of the functions  $U_\mp$  is rather cumbersome [28]. To our knowledge, Eqs. (8)-(9) have never been explicitly presented before. The expression for  $\Omega$  in terms of  $(\hat{r}, \hat{a}, \sigma)$  is given in Ref. [28].

In the EMRI limit the radiation-reaction time scale is much longer than the orbital period. We can therefore assume that the inspiral is adiabatic. Under this approximation the system evolves as the change in the binding energy is balanced by the total GW flux at infinity and at the horizon,  $-\dot{E}_{\text{orb}} = \dot{E}_{\text{GW}} = \dot{E}_{\text{GW}}^+ + \dot{E}_{\text{GW}}^-$ , where

$$\dot{E}_{\text{GW}}^- = \sum_{\ell m} \frac{|Z_{\ell m}^-|^2}{4\pi m^2 \Omega^2}, \quad \dot{E}_{\text{GW}}^+ = \sum_{\ell m} \frac{\alpha_{\ell m} |Z_{\ell m}^+|^2}{4\pi m^2 \Omega^2}, \quad (10)$$

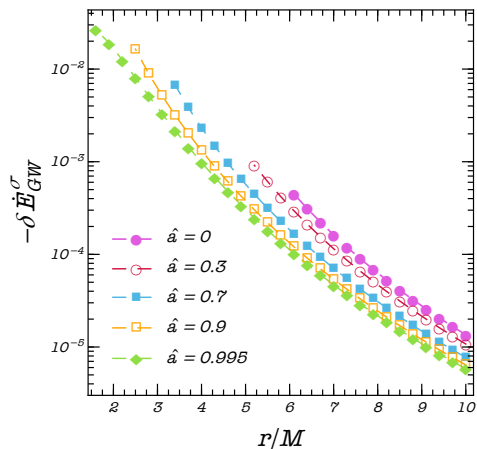


FIG. 1. The spin-correction coefficient  $\delta\dot{E}_{\text{GW}}^\sigma$  [see Eq. (11)] as a function of the orbital radius (up to the ISCO) for different values of the spin  $\hat{a} \equiv a/M$  of the primary.

and the coefficients  $\alpha_{\ell m}$  are given in Ref. [60]. We checked that for (anti)aligned spins circular equatorial orbits remain circular during the evolution [28, 59]. In our calculations we sum the multipole contributions up to  $\ell = 20$ ; truncation errors are 0.05% in the most extreme cases,  $\hat{a} = 0.995$  at the innermost stable circular orbit (ISCO), and typically much smaller [28].

In the adiabatic approximation a two-time scale analysis shows that during the EMRI evolution the masses and spins of the binary can be neglected to leading order [61]. The evolution of the spin of the secondary would introduce dissipative self-torque [62] which is anyway subdominant with respect to the effects discussed here.

**Results.** In the  $|\sigma| \ll 1$  limit, the GW flux can be expanded as

$$\dot{E}_{\text{GW}} = q^2 \left( \dot{E}_{\text{GW}}^0 + \sigma \delta\dot{E}_{\text{GW}}^\sigma + \mathcal{O}(\sigma^2) \right), \quad (11)$$

where we have factored out an overall mass-ratio dependence,  $\dot{E}_{\text{GW}}^0$  is the (normalized) flux for a nonspinning secondary, whereas  $\delta\dot{E}_{\text{GW}}^\sigma$  is the (normalized) spin contribution of the secondary. As anticipated, the latter is suppressed by a factor of  $\mathcal{O}(q)$  relative to the leading-order term. It therefore enters at the same order as the leading-order conservative part and the second-order dissipative part of the self-force [44, 63]. In Fig. 1 we show  $\delta\dot{E}_{\text{GW}}^\sigma$  as a function of the orbital radius. As expected the correction becomes stronger when the orbit approaches the ISCO and when the primary is rapidly spinning. A detailed analysis of the fluxes and a comparison with previous work [62, 64] is presented in Ref. [28].

With the fluxes  $\dot{E}_{\text{GW}}$  at hand, it is possible to calculate the evolution of the orbital radius  $r(t)$  and phase  $\Phi(t)$  due

to radiation losses. In the adiabatic approximation,

$$\frac{dr}{dt} = -\dot{E}_{\text{GW}}(r) \left( \frac{dE}{dr} \right)^{-1}, \quad \frac{d\Phi}{dt} = \Omega(r), \quad (12)$$

where  $E = \mu\hat{E}$  can be computed from Eq. (8), and  $\dot{E}_{\text{GW}}(r)$  is obtained by interpolating the calculated fluxes in the range  $r \in (r_{\text{start}}, r_{\text{ISCO}})$ . The starting point  $r_{\text{start}}$  is chosen such that the initial orbital frequency is the same as in the case of a nonspinning particle at the reference value  $r = 10.1M$ . Note that the ISCO location and frequency get  $\mathcal{O}(\sigma)$  corrections relative to the case of a nonspinning secondary [28, 65, 66].

By integrating the system (12) we can obtain the *instantaneous* orbital phase, which is related to the GW phase of the dominant mode by  $\Phi_{\text{GW}} = 2\Phi$ . The latter can be schematically written as

$$\Phi_{\text{GW}}(t) = \frac{1}{q} \left( \Phi_{\text{GW}}^0(t) + \sigma \delta\Phi_{\text{GW}}^\sigma(t) + \mathcal{O}(\sigma^2) \right), \quad (13)$$

where  $\Phi_{\text{GW}}^0(t)$  is the (normalized) phase for a nonspinning secondary,  $\delta\Phi_{\text{GW}}^\sigma(t)$  is the (normalized) spin correction, and we have factored out an overall  $q^{-1}$  dependence. As expected, the spin correction is suppressed by a factor of  $\mathcal{O}(q)$  and is therefore independent of  $q$  to the leading order, since the factor  $q^{-1}$  cancels out with  $\sigma$  [see Eq. (2)]. In the left panel of Fig. 2 we show  $\delta\Phi_{\text{GW}}^\sigma(t)$  and the spin correction to the *accumulated* GW phase,  $\Phi_{\text{GW}}^{\text{tot}} = \Phi_{\text{GW}}(t_{\text{ref}})$ , for some representative examples. As a reference, we chose the same  $t_{\text{ref}}$  for any value of  $\chi$ . In particular, we chose  $t_{\text{ref}}$  as the time to reach the ISCO for a nonspinning secondary minus 0.5 day, so that the evolution stops before the ISCO for any value of  $\chi$  and  $\hat{a}$ . A useful fit of the total accumulated GW phase is:

$$\delta\Phi_{\text{GW}}^\sigma(t_{\text{ref}}) = \sum_{i=0}^3 c_i (1 - \hat{a}^2)^{i/2} + c_4 \hat{a}, \quad (14)$$

where  $c_0 = 38.44, c_1 = -90.36, c_2 = 99.43, c_3 = -44.95, c_4 = 1.91$ . The fit is accurate within 5% in the whole range  $\hat{a} \in [0, 0.995]$ , with better accuracy at large  $\hat{a}$ .

**Measuring the spin of the secondary.** Parameter estimation for EMRIs is a challenging problem [31, 68] and a detailed analysis for the spin of the secondary will appear elsewhere. Here we estimate the potential to measure  $\chi$  by using a simple requirement: a total dephasing  $\approx 1$  rad or greater is likely to substantially impact a matched-filter search, leading to a significant loss of detected events [69].

Let us consider two waveforms which differ only by the value of the spin of the secondary,  $\chi_A$  and  $\chi_B$ , respectively. Using Eq. (13), the minimum difference  $\Delta\chi = \chi_B - \chi_A$  which would lead to a difference in phase at least of  $\alpha$  rad is:

$$|\Delta\chi| > \frac{\alpha}{|\delta\Phi_{\text{GW}}^\sigma|}. \quad (15)$$

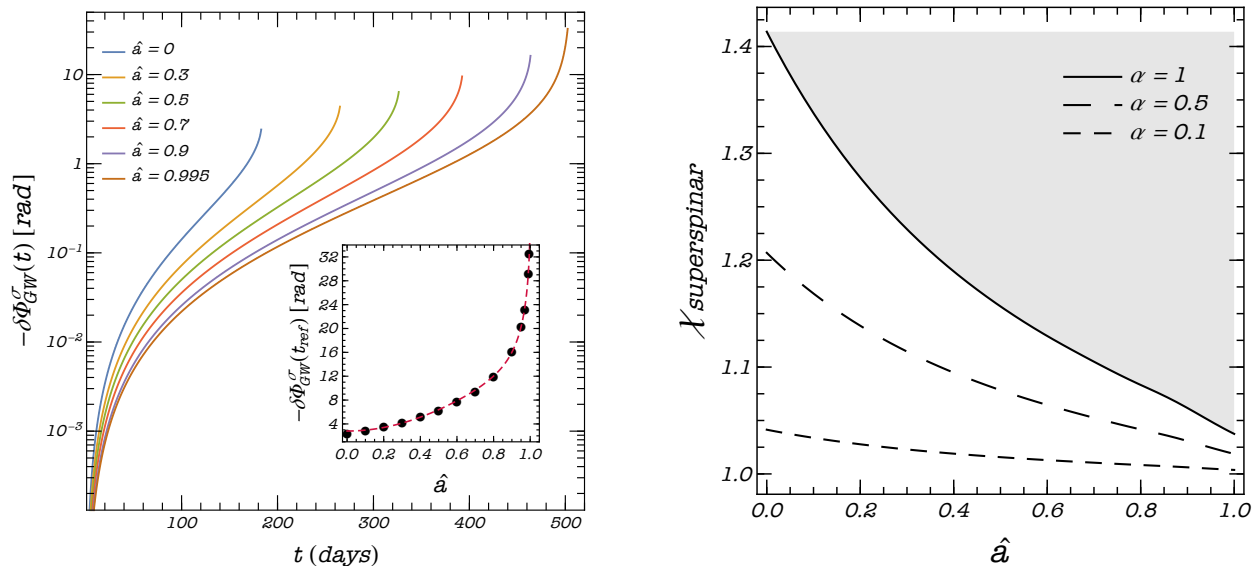


FIG. 2. Left panel: Spin correction,  $\delta\Phi_{\text{GW}}^\sigma(t)$ , to the instantaneous GW phase [cf. Eq. (13)] as a function of time up to the ISCO for different values of the spin  $\hat{a}$  of the primary. The inset shows the spin correction,  $\delta\Phi_{\text{GW}}^\sigma(t_{\text{ref}})$ , to the total accumulated phase. The dashed colored curve shows the fit (14). We assumed  $\mu = 30M_\odot$  and  $M = 10^6 M_\odot$  as reference values. Note that in general  $\delta\Phi_{\text{GW}}^\sigma(t_{\text{ref}}) < 0$ , i.e. when  $\chi > 0$  the inspiral lasts longer. Data are publicly available [67]. Right panel: Exclusion plot for the spin of a superspinner obtained using the criterion (15). A measured dephasing at the level of  $\alpha$  rad would exclude/probe the region above each curve.

For a reference value  $\hat{a} = 0.7$  ( $\hat{a} = 0.9$ ), with  $\alpha = 1$  rad [69], we obtain  $|\Delta\chi| > 0.1$  ( $|\Delta\chi| > 0.05$ ). Thus, our simplified analysis shows that EMRIs can provide a measurement of the spin of the secondary at the level of 5 – 10% for fastly spinning primaries. This adds to the outstanding accuracy in the measurements of  $M$ ,  $\mu$ , and  $\hat{a}$  [31]. More stringent constraints would arise by an analysis of the mismatch between two waveforms [41, 69, 70], which would suggest using  $\alpha < 1$  for our estimates.

In addition to providing an accurate and model-independent way to measure spins of stellar-mass objects, EMRI detections can provide theory-agnostic tests of the Kerr bound (1) and, in particular, of superspinars [45]. Indeed, since  $|\chi_A| \leq 1$  for a Kerr BH, an accuracy at the level of (say)  $|\Delta\chi| > 0.1$  allows us to distinguish a Kerr BH from a superspinner provided the spin of the latter is  $|\chi_B| \gtrsim 1 + |\Delta\chi| \approx 1.1$ . The right panel of Fig. 2 shows the exclusion plot for the spin of a superspinner obtained using the criterion (15) and under the most conservative assumption,  $\chi_A = 1$ , as a function of the spin  $\hat{a}$  of the primary. We consider different values for the dephasing threshold  $\alpha$ . For the standard choice of  $\alpha = 1$  rad, our results suggest that it should be possible to exclude/probe the range  $|\chi_B| > 1.4$  ( $|\chi_B| > 1.05$ ) for nonspinning (highly-spinning) primaries. Since no theoretical upper bound is expected for superspinars (other, possibly, than those coming from the ergoregion instability [71–73]) a spin measurement at this level can potentially probe a vast region of the parameter space for

these objects.

**Discussion.** EMRIs are unique probes of fundamental physics [16, 42]. Besides offering the opportunity for exquisite tests of gravity [34–39] and of the nature of supermassive objects [31, 33, 40, 41, 74], here we have shown that they can be used to perform theory-agnostic tests of the Kerr bound. Our results suggest that EMRI detections with LISA have the potential to rule out (or detect) superspinars almost in the entire region of the parameter space. This conclusion is based on a simplistic analysis, which must be validated with a more careful study, for example including accurate waveform models, a statistical analysis that can account for correlations among the waveform parameters, and the fact that LISA will be a signal-driven GW detector, so that numerous simultaneously-detected sources must be suitably subtracted [29, 68, 75].

No EMRI inspiral and waveform model is complete at post-adiabatic order without including the spin of the secondary along with first-order conservative and second-order dissipative self-force effects [62]. In addition with a more rigorous parameter estimation including also self-force effects, future work will focus on noncircular/nonequatorial orbits and on the case of misaligned spins, which introduces precession in the motion [59].

Finally, it would be very interesting to include higher multipole moments for the secondary, in particular the quadrupole moment. Although this effect is suppressed by a further  $\mathcal{O}(q)$  factor and is probably too small to be

detectable with LISA, it can potentially allow performing model-independent tests of the no-hair theorem on the secondary.

**Acknowledgments.** We thank Richard Brito and Niels Warburton for useful discussion. P.P. acknowledges financial support provided under the European Union’s H2020 ERC, Starting Grant agreement no. DarkGRA–757480, and under the MIUR PRIN and FARE programmes (GW-NEXT, CUP: B84I20000100001). The authors would like to acknowledge networking support by the COST Action CA16104 and support from the Amaldi Research Center funded by the MIUR program ”Dipartimento di Eccellenza” (CUP: B81I18001170001).

- 
- [1] R. Penrose, “Asymptotic properties of fields and space-times,” *Phys. Rev. Lett.* **10** (1963) 66–68.
- [2] R. Penrose, “Gravitational collapse and space-time singularities,” *Phys. Rev. Lett.* **14** (1965) 57–59.
- [3] J. A. Wheeler, “Our Universe: the known and the unknown,” *The Physics Teacher* **7** (1969) 1.
- [4] S. W. Hawking, “Black Holes and Thermodynamics,” *Phys. Rev.* **D13** (1976) 191–197.
- [5] J. D. Bekenstein, “Black holes and the second law,” *Lett. Nuovo Cim.* **4** (1972) 737–740.
- [6] J. D. Bekenstein, “Black holes and entropy,” *Phys. Rev.* **D7** (1973) 2333–2346.
- [7] B. Carter, “Hamilton-Jacobi and Schrodinger separable solutions of Einstein’s equations,” *Commun. Math. Phys.* **10** no. 4, (1968) 280–310.
- [8] B. Carter, “Global structure of the Kerr family of gravitational fields,” *Phys. Rev.* **174** (1968) 1559–1571.
- [9] C. M. Will, “The Confrontation between General Relativity and Experiment,” *Living Rev. Rel.* **17** (2014) 4, [arXiv:1403.7377 \[gr-qc\]](#).
- [10] N. Yunes, K. Yagi, and F. Pretorius, “Theoretical Physics Implications of the Binary Black-Hole Mergers GW150914 and GW151226,” *Phys. Rev.* **D94** no. 8, (2016) 084002, [arXiv:1603.08955 \[gr-qc\]](#).
- [11] **LIGO Scientific, Virgo** Collaboration, B. P. Abbott *et al.*, “Tests of general relativity with GW150914,” *Phys. Rev. Lett.* **116** no. 22, (2016) 221101, [arXiv:1602.03841 \[gr-qc\]](#). [Erratum: *Phys. Rev. Lett.* 121,no.12,129902(2018)].
- [12] We use geometric units,  $G = c = 1$ , and we define the Riemann tensor as  $R_{\mu\nu\sigma}{}^{\delta}\omega_{\delta} = 2\nabla_{[\mu}\nabla_{\nu]}\omega_{\sigma}$ , where  $\nabla_{\mu}$  is the covariant derivative and  $\omega_{\delta}$  an arbitrary 1-form, while the square brackets denotes the antisymmetrization. This is the same notation adopted in the package xCOBA of the software MATHEMATICA, which we used for all tensor computation. The metric signature is  $(-, +, +, +)$ .
- [13] C. Bambi, “Testing the Kerr black hole hypothesis,” *Mod. Phys. Lett.* **A26** (2011) 2453–2468, [arXiv:1109.4256 \[gr-qc\]](#).
- [14] E. Berti *et al.*, “Testing General Relativity with Present and Future Astrophysical Observations,” *Class. Quant. Grav.* **32** (2015) 243001, [arXiv:1501.07274 \[gr-qc\]](#).
- [15] K. Yagi and L. C. Stein, “Black Hole Based Tests of General Relativity,” *Class. Quant. Grav.* **33** no. 5, (2016) 054001, [arXiv:1602.02413 \[gr-qc\]](#).
- [16] L. Barack *et al.*, “Black holes, gravitational waves and fundamental physics: a roadmap,” *Class. Quant. Grav.* **36** no. 14, (2019) 143001, [arXiv:1806.05195 \[gr-qc\]](#).
- [17] V. Cardoso and P. Pani, “Testing the nature of dark compact objects: a status report,” *Living Rev. Rel.* **22** no. 1, (2019) 4, [arXiv:1904.05363 \[gr-qc\]](#).
- [18] F. D. Ryan, “Spinning boson stars with large selfinteraction,” *Phys. Rev.* **D55** (1997) 6081–6091.
- [19] P. Pani, C. F. B. Macedo, L. C. B. Crispino, and V. Cardoso, “Slowly rotating black holes in alternative theories of gravity,” *Phys. Rev.* **D84** (2011) 087501, [arXiv:1109.3996 \[gr-qc\]](#).
- [20] B. Kleihaus, J. Kunz, and E. Radu, “Rotating Black Holes in Dilatonic Einstein-Gauss-Bonnet Theory,” *Phys. Rev. Lett.* **106** (2011) 151104, [arXiv:1101.2868 \[gr-qc\]](#).
- [21] C. A. R. Herdeiro and E. Radu, “Kerr black holes with scalar hair,” *Phys. Rev. Lett.* **112** (2014) 221101, [arXiv:1403.2757 \[gr-qc\]](#).
- [22] D. Ayzenberg and N. Yunes, “Slowly-Rotating Black Holes in Einstein-Dilaton-Gauss-Bonnet Gravity: Quadratic Order in Spin Solutions,” *Phys. Rev.* **D90** (2014) 044066, [arXiv:1405.2133 \[gr-qc\]](#). [Erratum: *Phys. Rev.* D91,no.6,069905(2015)].
- [23] A. Maselli, P. Pani, L. Gualtieri, and V. Ferrari, “Rotating black holes in Einstein-Dilaton-Gauss-Bonnet gravity with finite coupling,” *Phys. Rev.* **D92** no. 8, (2015) 083014, [arXiv:1507.00680 \[gr-qc\]](#).
- [24] E. Barausse, T. P. Sotiriou, and I. Vega, “Slowly rotating black holes in Einstein-ther theory,” *Phys. Rev.* **D93** no. 4, (2016) 044044, [arXiv:1512.05894 \[gr-qc\]](#).
- [25] C. Herdeiro, E. Radu, and H. Rnarrson, “Kerr black holes with Proca hair,” *Class. Quant. Grav.* **33** no. 15, (2016) 154001, [arXiv:1603.02687 \[gr-qc\]](#).
- [26] P. V. P. Cunha, C. A. R. Herdeiro, and E. Radu, “Spontaneously Scalarized Kerr Black Holes in Extended Scalar-TensorGauss-Bonnet Gravity,” *Phys. Rev. Lett.* **123** no. 1, (2019) 011101, [arXiv:1904.09997 \[gr-qc\]](#).
- [27] A. Maselli, H. O. Silva, M. Minamitsuji, and E. Berti, “Slowly rotating black hole solutions in Horndeski gravity,” *Phys. Rev.* **D92** no. 10, (2015) 104049, [arXiv:1508.03044 \[gr-qc\]](#).
- [28] G. A. Piovano, A. Maselli, and P. Pani, “Extreme mass ratio inspirals with spinning secondary: a detailed study of equatorial, circular motion,” *in preparation*.
- [29] **LISA** Collaboration, P. Amaro-Seoane *et al.*, “Laser Interferometer Space Antenna,” [arXiv:1702.00786 \[astro-ph.IM\]](#).
- [30] V. Baibhav *et al.*, “Probing the Nature of Black Holes: Deep in the mHz Gravitational-Wave Sky,” [arXiv:1908.11390 \[astro-ph.HE\]](#).
- [31] S. Babak, J. Gair, A. Sesana, E. Barausse, C. F. Sopuerta, C. P. L. Berry, E. Berti, P. Amaro-Seoane, A. Petiteau, and A. Klein, “Science with the space-based interferometer LISA. V: Extreme mass-ratio inspirals,” *Phys. Rev.* **D95** no. 10, (2017) 103012, [arXiv:1703.09722 \[gr-qc\]](#).
- [32] K. Glampedakis and S. Babak, “Mapping spacetimes with LISA: Inspiral of a test-body in a ‘quasi-Kerr’ field,” *Class. Quant. Grav.* **23** (2006) 4167–4188, [arXiv:gr-qc/0510057 \[gr-qc\]](#).
- [33] L. Barack and C. Cutler, “Using LISA EMRI sources to

- test off-Kerr deviations in the geometry of massive black holes,” *Phys. Rev.* **D75** (2007) 042003, [arXiv:gr-qc/0612029 \[gr-qc\]](#).
- [34] C. F. Sopuerta and N. Yunes, “Extreme and Intermediate-Mass Ratio Inspirals in Dynamical Chern-Simons Modified Gravity,” *Phys. Rev.* **D80** (2009) 064006, [arXiv:0904.4501 \[gr-qc\]](#).
- [35] N. Yunes, P. Pani, and V. Cardoso, “Gravitational Waves from Quasicircular Extreme Mass-Ratio Inspirals as Probes of Scalar-Tensor Theories,” *Phys. Rev.* **D85** (2012) 102003, [arXiv:1112.3351 \[gr-qc\]](#).
- [36] P. Pani, V. Cardoso, and L. Gualtieri, “Gravitational waves from extreme mass-ratio inspirals in Dynamical Chern-Simons gravity,” *Phys. Rev.* **D83** (2011) 104048, [arXiv:1104.1183 \[gr-qc\]](#).
- [37] E. Barausse, N. Yunes, and K. Chamberlain, “Theory-Agnostic Constraints on Black-Hole Dipole Radiation with Multiband Gravitational-Wave Astrophysics,” *Phys. Rev. Lett.* **116** no. 24, (2016) 241104, [arXiv:1603.04075 \[gr-qc\]](#).
- [38] K. Chamberlain and N. Yunes, “Theoretical Physics Implications of Gravitational Wave Observation with Future Detectors,” *Phys. Rev.* **D96** no. 8, (2017) 084039, [arXiv:1704.08268 \[gr-qc\]](#).
- [39] V. Cardoso, G. Castro, and A. Maselli, “Gravitational waves in massive gravity theories: waveforms, fluxes and constraints from extreme-mass-ratio mergers,” *Phys. Rev. Lett.* **121** no. 25, (2018) 251103, [arXiv:1809.00673 \[gr-qc\]](#).
- [40] P. Pani and A. Maselli, “Love in Extrema Ratio,” *Int. J. Mod. Phys.* **D28** no. 14, (2019) 1944001, [arXiv:1905.03947 \[gr-qc\]](#).
- [41] S. Datta, R. Brito, S. Bose, P. Pani, and S. A. Hughes, “Tidal heating as a discriminator for horizons in extreme mass ratio inspirals,” *Phys. Rev.* **D101** no. 4, (2020) 044004, [arXiv:1910.07841 \[gr-qc\]](#).
- [42] E. Barausse *et al.*, “Prospects for Fundamental Physics with LISA,” [arXiv:2001.09793 \[gr-qc\]](#).
- [43] E. Poisson, “The Motion of point particles in curved space-time,” *Living Rev. Rel.* **7** (2004) 6, [arXiv:gr-qc/0306052 \[gr-qc\]](#).
- [44] L. Barack, “Gravitational self force in extreme mass-ratio inspirals,” *Class. Quant. Grav.* **26** (2009) 213001, [arXiv:0908.1664 \[gr-qc\]](#).
- [45] E. G. Gimon and P. Horava, “Astrophysical violations of the Kerr bound as a possible signature of string theory,” *Phys. Lett.* **B672** (2009) 299–302, [arXiv:0706.2873 \[hep-th\]](#).
- [46] If superspinars arise in modified gravity, the high-energy corrections would occur at high curvature. Therefore the modification to the metric of the primary are subleading compared to those of the secondary, which justifies our assumption of a Kerr background.
- [47] M. Mathisson, “Neue mechanik materieller systemes,” *Acta Phys. Polon.* **6** (1937) 163–2900.
- [48] A. Papapetrou, “Spinning test particles in general relativity. 1.,” *Proc. Roy. Soc. Lond.* **A209** (1951) 248–258.
- [49] E. Corinaldesi and A. Papapetrou, “Spinning test particles in general relativity. 2.,” *Proc. Roy. Soc. Lond.* **A209** (1951) 259–268.
- [50] W. Tulczyjew, “Motion of multipole particles in general relativity theory,” *Acta Phys. Pol.* **18** (1959) 393.
- [51] W. Dixon, “A covariant multipole formalism for extended test bodies in general relativity,” *Il Nuovo Cimento* **34** no. 2, (Oct, 1964) 317–339.
- [52] W. G. Dixon, “Dynamics of extended bodies in general relativity. I. Momentum and angular momentum,” *Proc. Roy. Soc. Lond.* **A314** (1970) 499–527.
- [53] W. G. Dixon, “Dynamics of extended bodies in general relativity. II. Moments of the charge-current vector,” *Proc. Roy. Soc. Lond.* **A319** (1970) 509–547.
- [54] J. Steinhoff and D. Puetzfeld, “Multipolar equations of motion for extended test bodies in General Relativity,” *Phys. Rev.* **D81** (2010) 044019, [arXiv:0909.3756 \[gr-qc\]](#).
- [55] K. Kyriani and O. Semerak, “Spinning test particles in a Kerr field,” *Mon. Not. Roy. Astron. Soc.* **382** (2007) 1922.
- [56] This condition reflects the physical requirement that particles with intrinsic angular momentum must have a finite size in classical theories.
- [57] S. Drasco and S. A. Hughes, “Gravitational wave snapshots of generic extreme mass ratio inspirals,” *Phys. Rev.* **D73** no. 2, (2006) 024027, [arXiv:gr-qc/0509101 \[gr-qc\]](#). [Erratum: *Phys. Rev.* **D88**, no. 10, 109905 (2013); Erratum: *Phys. Rev.* **D90**, no. 10, 109905 (2014)].
- [58] S. A. Hughes, “The Evolution of circular, nonequatorial orbits of Kerr black holes due to gravitational wave emission,” *Phys. Rev.* **D61** no. 8, (2000) 084004, [arXiv:gr-qc/9910091 \[gr-qc\]](#). [Erratum: *Phys. Rev.* **D63**, no. 4, 049902 (2001); Erratum: *Phys. Rev.* **D65**, no. 6, 069902 (2002); Erratum: *Phys. Rev.* **D67**, no. 8, 089901 (2003); Erratum: *Phys. Rev.* **D78**, no. 10, 109902 (2008); Erratum: *Phys. Rev.* **D90**, no. 10, 109904 (2014)].
- [59] T. Tanaka, Y. Mino, M. Sasaki, and M. Shibata, “Gravitational waves from a spinning particle in circular orbits around a rotating black hole,” *Phys. Rev.* **D54** (1996) 3762–3777, [arXiv:gr-qc/9602038 \[gr-qc\]](#).
- [60] A. Taracchini, A. Buonanno, S. A. Hughes, and G. Khanna, “Modeling the horizon-absorbed gravitational flux for equatorial-circular orbits in Kerr spacetime,” *Phys. Rev.* **D88** (2013) 044001, [arXiv:1305.2184 \[gr-qc\]](#). [Erratum: *Phys. Rev.* **D88**, no. 10, 109903 (2013)].
- [61] T. Hinderer and E. E. Flanagan, “Two timescale analysis of extreme mass ratio inspirals in Kerr. I. Orbital Motion,” *Phys. Rev.* **D78** (2008) 064028, [arXiv:0805.3337 \[gr-qc\]](#).
- [62] N. Afcay, S. R. Dolan, C. Kavanagh, J. Moxon, N. Warburton, and B. Wardell, “Dissipation in extreme-mass ratio binaries with a spinning secondary,” [arXiv:1912.09461 \[gr-qc\]](#).
- [63] A. Pound, “Second-order gravitational self-force,” *Phys. Rev. Lett.* **109** (2012) 051101, [arXiv:1201.5089 \[gr-qc\]](#).
- [64] E. Harms, G. Lukes-Gerakopoulos, S. Bernuzzi, and A. Nagar, “Asymptotic gravitational wave fluxes from a spinning particle in circular equatorial orbits around a rotating black hole,” *Phys. Rev.* **D93** no. 4, (2016) 044015, [arXiv:1510.05548 \[gr-qc\]](#). [Addendum: *Phys. Rev.* **D100**, no. 12, 129901 (2019)].
- [65] J. Steinhoff and D. Puetzfeld, “Influence of internal structure on the motion of test bodies in extreme mass ratio situations,” *Phys. Rev.* **D86** (2012) 044033, [arXiv:1205.3926 \[gr-qc\]](#).

- [66] P. I. Jefremov, O. Yu. Tsupko, and G. S. Bisnovaty-Kogan, “Innermost stable circular orbits of spinning test particles in Schwarzschild and Kerr space-times,” *Phys. Rev.* **D91** no. 12, (2015) 124030, [arXiv:1503.07060 \[gr-qc\]](#).
- [67] Data and relevant codes are publicly available at <https://web.uniroma1.it/gmunu>.
- [68] A. J. K. Chua, N. Korsakova, C. J. Moore, J. R. Gair, and S. Babak, “Gaussian processes for the interpolation and marginalization of waveform error in extreme-mass-ratio-inspiral parameter estimation,” *Phys. Rev.* **D101** no. 4, (2020) 044027, [arXiv:1912.11543 \[astro-ph.IM\]](#).
- [69] L. Lindblom, B. J. Owen, and D. A. Brown, “Model Waveform Accuracy Standards for Gravitational Wave Data Analysis,” *Phys. Rev.* **D78** (2008) 124020, [arXiv:0809.3844 \[gr-qc\]](#).
- [70] E. E. Flanagan and S. A. Hughes, “Measuring gravitational waves from binary black hole coalescences: 2. The Waves’ information and its extraction, with and without templates,” *Phys. Rev.* **D57** (1998) 4566–4587, [arXiv:gr-qc/9710129 \[gr-qc\]](#).
- [71] P. Pani, E. Barausse, E. Berti, and V. Cardoso, “Gravitational instabilities of superspinars,” *Phys. Rev.* **D82** (2010) 044009, [arXiv:1006.1863 \[gr-qc\]](#).
- [72] E. Maggio, P. Pani, and V. Ferrari, “Exotic Compact Objects and How to Quench their Ergoregion Instability,” *Phys. Rev.* **D96** no. 10, (2017) 104047, [arXiv:1703.03696 \[gr-qc\]](#).
- [73] R. Roy, P. Kocherlakota, and P. S. Joshi, “Mode stability of a near-extremal Kerr superspinar,” [arXiv:1911.06169 \[gr-qc\]](#).
- [74] P. Pani, E. Berti, V. Cardoso, Y. Chen, and R. Norte, “Gravitational-wave signatures of the absence of an event horizon. II. Extreme mass ratio inspirals in the spacetime of a thin-shell gravastar,” *Phys. Rev.* **D81** (2010) 084011, [arXiv:1001.3031 \[gr-qc\]](#).
- [75] LISA Data Challenge Working Group. LISA Data Challenges, 2019. <https://lisa-ldc.lal.in2p3.fr>.